

# Nitrogen and Phosphorus Codoped Porous Carbon Framework as Anode Material for High Rate Lithium-Ion Batteries

Chunrong Ma,<sup>†</sup> Changjian Deng,<sup>‡</sup> XiaoZhen Liao,<sup>†</sup> YuShi He,<sup>†</sup> ZiFeng Ma,<sup>\*,†,§</sup> and Hui Xiong<sup>\*,‡</sup>

<sup>†</sup>Shanghai Electrochemical Energy Devices Research Centre, School of Chemistry and Chemical Engineering, Shanghai Jiao Tong University, Shanghai 200240, China

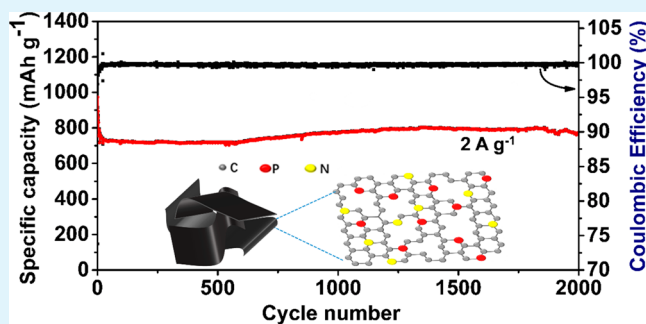
<sup>‡</sup>Micrometer School of Materials Science and Engineering, Boise State University, Boise, Idaho 83725, United States

<sup>§</sup>Sinopoly Battery Research Centre, Shanghai 200241, China

## S Supporting Information

**ABSTRACT:** Slow kinetics and low specific capacity of graphite anode significantly limit its applications in the rapidly developing lithium-ion battery (LIB) markets. Herein, we report a carbon framework anode with ultrafast rate and cycling stability for LIBs by nitrogen and phosphorus doping. The electrode structure is constructed of a 3D framework built from 2D heteroatom-doped graphene layers via pyrolysis of self-assembled supramolecular aggregates. The synergistic effect from the nanostructured 3D framework and chemical doping (i.e., N- and P-doping) enables fast kinetics in charge storage and transport. A high reversible capacity of 946 mAh g<sup>-1</sup> is delivered at a current rate of 0.5 A g<sup>-1</sup>, and excellent rate capability (e.g., a capacity of 595 mAh g<sup>-1</sup> at 10 A g<sup>-1</sup>) of the electrode is shown. Moreover, a moderate surface area from the 3D porous structure contributes to a relatively high initial Coulombic efficiency of 74%, compared to other graphene-based anode materials. The electrode also demonstrates excellent cycling stability at a current rate of 2 A g<sup>-1</sup> for 2000 cycles. The synthetic strategy proposed here is highly efficient and green, which can provide guidance for large-scale controllable fabrication of carbon-based anode materials.

**KEYWORDS:** lithium-ion batteries, 3D porous carbon framework, nanoarchitecture, N- and P-doping, high rate



## 1. INTRODUCTION

The rechargeable lithium-ion battery (LIB) has been the leading practical energy storage technology and dominated portable electronic markets since it was commercialized by Sony in the 1990s.<sup>1–3</sup> In recent years, the hurdles for LIB developments include limited energy, power density, and cycling stability, which hindered their applications in powering next-generation electric vehicles for ultrafast charging. Graphite is the state-of-the-art anode material for LIBs. However, its low theoretical specific capacity and inferior rate capability have limited its high energy/power applications. The intercalation process in graphite anode is diffusion-limited. At fast charge rates Li<sup>+</sup> will deposit or plate as Li metal on the graphite surface where mass transfer by diffusion cannot be sustained at high currents, which eventually leads to capacity loss, dendrite growth, increased resistance, and thermal runaways. To reach the desired performance targets, it is critical to develop an anode material with fast kinetics. Significant efforts have been contributed to acquire high energy/power density electrodes by developing various alternatives to graphite anodes including hard carbon,<sup>4–8</sup> carbon black,<sup>9–11</sup> carbon fiber,<sup>12–14</sup> carbon nanotube,<sup>15–17</sup> and graphene.<sup>18–20</sup> Nevertheless, the aforementioned carbonaceous materials have issues of low initial

Coulombic efficiency or poor rate performance. Therefore, there still remains a grand challenge to fulfill the carbonaceous anode with both cycle life and rate capability for LIBs.

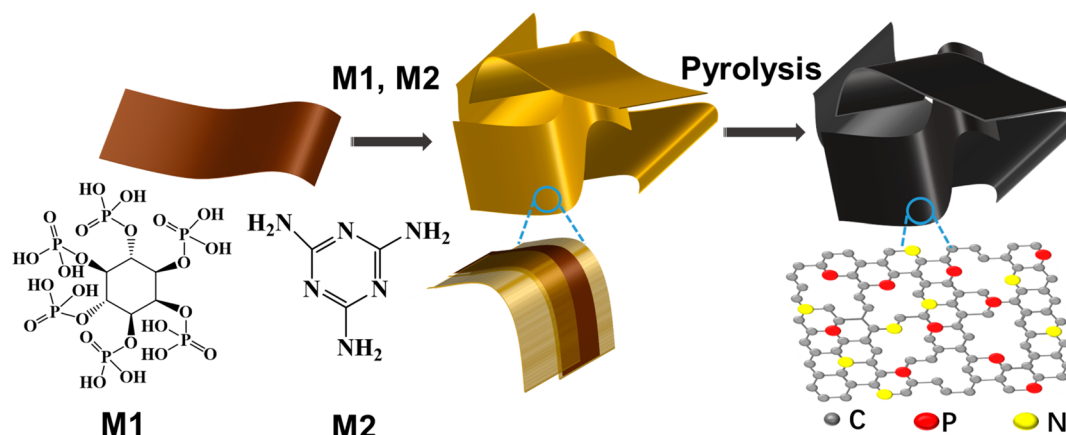
To improve the kinetics for a better rate performance, two-dimensional (2D) materials (e.g., graphene-based materials) have emerged as attractive solutions, owing to their superior electrical conductivity, high specific surface area, and short ion transport length.<sup>21,22</sup> Particularly, 2D ultrathin layer structures have the ability to improve storage capacity by binding Li ions not only on nanosheet surface but also on the edges and defects of the nanosheets.<sup>23,24</sup> Doping the material with lightweight heteroatoms (e.g., B, N, P, and S) is another useful strategy to improve the electrochemical performance of carbonaceous materials. Chemical doping in carbonaceous electrode materials can expand at specific areas to increase binding sites and further enhance the electrical conductivity to facilitate the charge transfer and transport process and therefore significantly improve the Li<sup>+</sup> storage and transport properties. In particular, N-doped carbon materials<sup>25–30</sup> have

Received: July 20, 2018

Accepted: October 1, 2018

Published: October 1, 2018

Scheme 1. Synthesis of NP-C (M1: Phytic Acid; M2: Melamine)



been investigated extensively and demonstrated an enhancement in electrochemical performance as anode materials for LIBs. Doping with phosphorus (P), which is in the same family as N, shows a higher electron-donating ability and stronger n-type behavior compared to N-doping. When assessing the synergistic effect of heteroatomic doping, N/P-codoping is a feasible strategy to distinguish electrodes with higher electronic conductivity and larger interlayer distance.

Herein, a N,P-doped porous carbon (NP-C) is synthesized, which consists of 2D ultrathin heteroatom-doped carbon layers via an *in situ* polymerization reaction, followed by calcination. Taking the advantages from 3D nanostructure and heteroatom doping, the optimized NP-C with enlarged interlayer distance demonstrates improved reaction kinetics for charge transfer and transport, indicated by the superior rate capability of 595 mAh g<sup>-1</sup> at a high current rate of 10 A g<sup>-1</sup>. Meanwhile, a high reversible capacity of 980 mAh g<sup>-1</sup> as well as a relatively high initial Coulombic efficiency (74%) can be reached at a current rate of 0.5 A g<sup>-1</sup> by offering more active Li<sup>+</sup> storage sites in NP-C. The Li<sup>+</sup> diffusivity of the NP-C electrode is estimated by the galvanostatic intermittent titration technique (GITT), indicating a high Li<sup>+</sup> diffusion. Besides, the charge storage mechanism of the NP-C electrode is investigated using cyclic voltammetry with varying scan rates. It is suggested that the pseudocapacitance due to surface redox reactions from defects, edges, and pores uniquely designed in this structure has a significant contribution to the overall charge storage.

## 2. EXPERIMENTAL SECTION

The modified Hummer's method<sup>31</sup> is used to produce graphene oxide (GO). In a typical process, 1.5 mL of phytic acid (70%, Aladdin) is mixed with GO solution under stirring, followed by the addition of 0.45 g of melamine (99%, Aladdin) into the solution, yielding a brown product. The product is collected by centrifugation, thoroughly washed with ethanol and DI water, and freeze-dried overnight. The final product is obtained by thermal treatment at 800 °C for 1 h at a ramp rate of 5 °C min<sup>-1</sup>.

A slurry of the active material, Super P, and polyvinylidene difluoride with a weight ratio of 8:1:1 is prepared, coated on a copper current collector, and transferred to a vacuum oven at 100 °C for 8 h. The loading density of the active material was ~1 mg cm<sup>-2</sup>. The 2016 coin cells are assembled with Li metal as the counter electrode and the electrolyte of 1 M LiPF<sub>6</sub> in dimethyl carbonate and ethylene carbonate (1:1 vol %). The electrochemical performance, cyclic voltammetry (CV), and electrochemical impedance spectroscopy (EIS) are conducted on the Land Battery Measurement System at a

potential window of 0.01–3 V, CHI605D electrochemical workstation, and AUTOLAB, respectively.

The morphology of the sample is characterized by scanning electron microscopy (SEM) on a HITACHI S-4800 and transmission electron microscopy (TEM) on a FEI Tecnai G2 with the accelerating voltage of 200 kV. X-ray diffraction (XRD) with Cu radiation was performed on a Dmax 2500 V to investigate the crystalline structure. X-ray photoelectron spectroscopy (XPS) scans are performed on an ESCALAB 250 photoelectron spectrometer. Raman spectra are collected by a Lab RAM HR800. The Brunner–Emmet–Teller (BET) surface area of the sample is measured on a Micromeritics ASAP 2020 analyzer. Four-point probe measurement (DP-SB100A/20) is performed to characterize the electric conductivity of the samples.

## 3. RESULTS AND DISCUSSION

The NP-C is synthesized via a facile method, as illustrated in Scheme 1. First, GO (Figure S1, Supporting Information) and melamine are dispersed in DI water with sonication at room temperature to form a homogeneous solution. Then phytic acid is added into the solution, and supramolecular aggregates are generated simultaneously on both sides of the GO surface, initiating the self-assembly of GO into a three-dimensional porous structure. Finally, the products are collected by centrifugation and annealed under Ar atmosphere. SEM and TEM are used to investigate the morphology and structure of the NP-C. From Figure 1a, an interconnected framework of

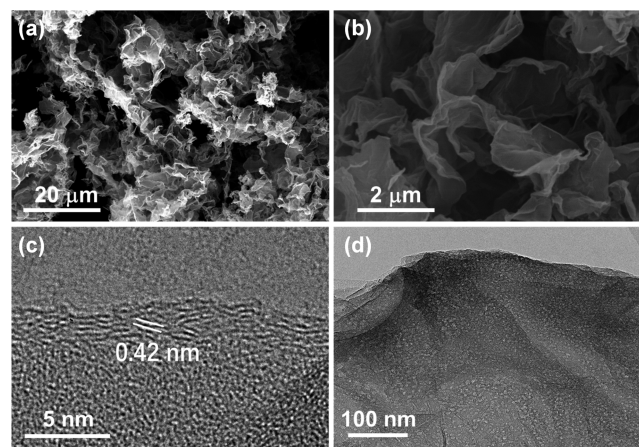


**Figure 1.** (a) Low-magnification SEM image for NP-C and (b) high-magnification SEM image for NP-C. (c, d) TEM images of NP-C.

ultrathin nanosheets with a high degree of porosity are visible. The carbon sheets with several micrometers in length can be clearly observed from Figure 1b, which are interconnected at the edges. The high-resolution TEM (HRTEM) image shown in Figure 1c demonstrates that each layered carbon sheet exhibits a wrinkled structure and multilayered domains at the edges with a spacing of  $\sim 0.42$  nm. The expanded  $d$  spacing is in favor of  $\text{Li}^+$  diffusion and storage from a previous report.<sup>32</sup> In addition, it can be seen that many pores exist on the surface of NP-C (Figure 1d). These pores not only can adsorb more  $\text{Li}^+$  for increased charge storage but also relieve the stress from the volume variation upon cycling, which improves the cycling stability.<sup>33</sup> Based on the images shown in Figure 1, the simultaneously grown carbon layer covers evenly on the surface of the graphene framework, and free carbon particles are not observed from either the TEM or SEM images. The element mapping images (Figure S2) further support the homogeneous distribution of nitrogen and phosphorus on the 3D carbon framework.

To obtain further insights into the structure of the NP-C, XRD is performed. There exhibits a peak at  $23.4^\circ$  (Figure 2a),

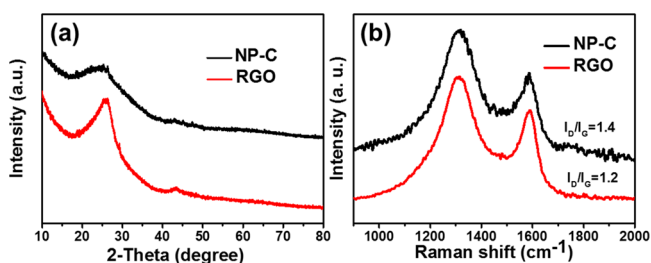


**Figure 2.** (a) XRD and (b) Raman spectra of the NP-C and RGO electrode.

corresponding to the graphitic (002) plane. Compared to the RGO sample, this peak is shifted to the left, implying that the N- and P-doping enlarge the interlayer distance as a result of the larger covalent radius of N and P atoms.<sup>34</sup> From the Raman spectrum displayed in Figure 2b, two distinct peaks located at  $\sim 1350$  and  $\sim 1590$   $\text{cm}^{-1}$  correspond to the D band (disordered  $\text{sp}^2$  carbon) and G band (graphitic  $\text{sp}^2$  carbons), respectively. The ratio of  $I_D/I_G$  reflects the degree of disorder of the materials. Compared to RGO ( $I_D/I_G = 1.2$ ), NP-C demonstrates a higher  $I_D/I_G$  (1.4), suggesting more disorder or defects as a result of the introduction of N and P.<sup>35,36</sup> The doping level and chemical state of the as-prepared NP-C are determined using XPS. The result demonstrates successful doping of N (15.18%) and P (9.33%) in NP-C. As shown in Figure 3a, peaks at  $\sim 132.8$  and  $\sim 399.5$  eV correspond to P 2p and N 1s, respectively. The high-resolution C 1s spectrum can be resolved into three individual peaks (Figure 3b), which are assigned to the  $\text{sp}^2$  C (284.8 eV), the C–N (286.5 eV), and O–C=O bond (287.8 eV), respectively. The N 1s spectrum (Figure 3c) is fitted to three peaks, corresponding to the pyridinic-N, pyrrolic-N, and oxidized N, respectively. From the high-resolution P 2p spectrum (Figure 3d), two fitting peaks are observed, ascribing to the P–C (131.6 eV) and P–O bond (133.2 eV),<sup>37</sup> respectively. The introduction of nitrogen and phosphorus can significantly improve the electronic conductivity of graphene. As expected, the electrical conductivity of NP-C is improved by up to 4 orders of magnitude ( $40 \text{ S m}^{-1}$ ), facilitating fast electron transport. Figure S3 shows the

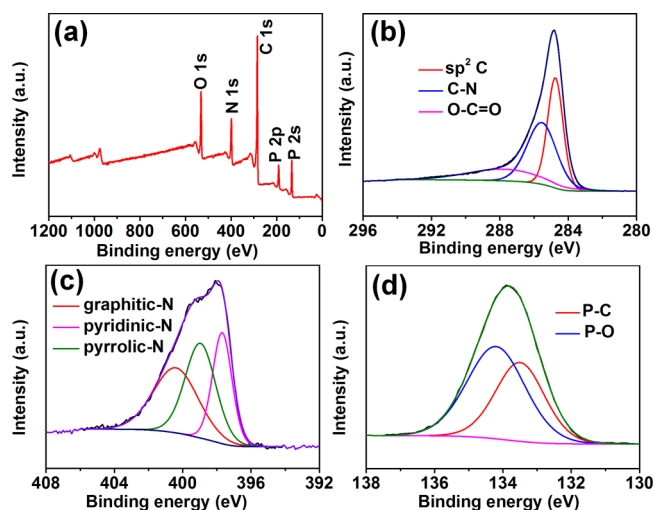


**Figure 3.** XPS spectra of NP-C: (a) survey spectrum of the NP-C and XPS high-resolution spectra of (b) C 1s, (c) N 1s, and (d) P 2p of the NP-C.

$\text{N}_2$  adsorption–desorption isotherm of NP-C sample, exhibiting a typical IV isotherm. The corresponding BET area of the NP-C is  $689 \text{ m}^2 \text{ g}^{-1}$ , which offers large space and channels for the  $\text{Li}^+$  diffusion to promote the rate capability through the surface-induced capacitance behavior. The corresponding pore size distribution curve reveals the presence of mesopores centered at around 3–4 nm.

The charge–discharge voltage profiles are presented in Figure 4a at a current density of  $0.5 \text{ A g}^{-1}$ . In the first cycle, the

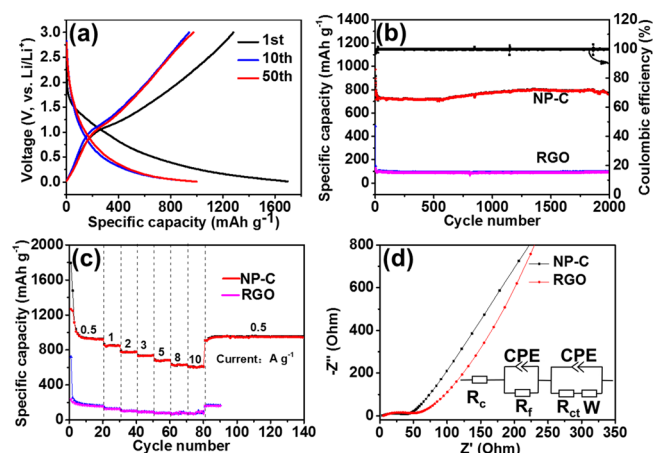


**Figure 4.** (a) Charge–discharge voltage profiles. (b) Long-term cycling performance of the NP-C electrode at a current of  $2 \text{ A g}^{-1}$ . (c) Rate performance of the NP-C electrode. (d) Nyquist plots of the NP-C and RGO electrodes (inset: Randles equivalent circuit model).

NP-C electrode shows a  $1695 \text{ mAh g}^{-1}$  discharge capacity and a  $1250 \text{ mAh g}^{-1}$  charge capacity, yielding an initial Coulombic efficiency (ICE) of 74%. The ICE of NP-C is better than the most recently reported carbon anode materials.<sup>8,18,38–41</sup> The improved ICE is attributed to the moderate surface area of NP-C. Additionally, P is more inclined to be incorporated into carbonaceous materials at the edge-plane sites owing to its larger size,<sup>35</sup> which facilitates the electron transport within the carbon materials as well as render better reversibility as less  $\text{Li}^+$  will be trapped. In the first cycle, the corresponding capacity loss is caused by the solid electrolyte interphase (SEI)

formation<sup>42–44</sup> as well as the irreversible insertion of Li<sup>+</sup> into special sites on highly defective and porous electrode.<sup>45</sup> From the 10th cycle, the discharge–charge profiles overlap in subsequent cycles, indicating that the formed SEI films are stabilized. The cycling performance of the NP-C electrode are also evaluated. As shown in Figure 4b, the NP-C electrode demonstrates a high reversible capacity of 740 mAh g<sup>-1</sup> even at a high current rate of 2 A g<sup>-1</sup> and a Coulombic efficiency of ~99–99.8%. The capacity decay is minimal after 2000 cycles, which is superior to that of the undoped RGO electrode under the same conditions.

To evaluate the power performance of the NP-C electrode, the rate capability is performed at various current rates. The NP-C electrode demonstrates high capacity and superior stability even at fast charge/discharge rates (Figure 4c). The high reversible capacity of 946, 812, 790, 743, 702, and 612 mAh g<sup>-1</sup> is delivered at a current density of 0.5, 1, 2, 3, 5, and 8 A g<sup>-1</sup>, respectively. The rate is then further increased to 10 A g<sup>-1</sup>, corresponding to a charge time of 30 s. A reversible capacity of 595 mAh g<sup>-1</sup> still can be achieved, indicating that this electrode has an ultrahigh rate capability. Furthermore, the NP-C electrode shows excellent reversibility and stability after deep charge/discharge cycling; a high reversible capacity of 980 mAh g<sup>-1</sup> can be recovered when the current density is set back to 0.5 A g<sup>-1</sup>. In contrast, the reversible capacities for RGO electrode are 198 and 98 mAh g<sup>-1</sup> at 0.5 and 5 A g<sup>-1</sup>, respectively, which are markedly lower than those from the NP-C electrode. The excellent performance of NP-C in terms of reversibility, cycling stability, and rate capability can allow NP-C to play critical roles in high-power LIB applications.

The kinetics of the NP-C and RGO electrode is studied using EIS. The Nyquist plots (Figure 4d) of NP-C and RGO electrodes have similar features. In specific, the fitting results of the impedance spectra using an equivalent circuit model consist of two semicircles at high and medium frequency range and a straight line at low frequency region. The first semicircles (at high frequency) is ascribed to the Li<sup>+</sup> migration through surface films ( $R_f$ ), the second semicircle (at medium frequency) is attributed to the interfacial charge transfer ( $R_{ct}$ ), and double-layer capacitance, while a straight line (at low frequency) region is concerned with the Li<sup>+</sup> diffusion process in the bulk materials ( $Z_w$ ).<sup>46</sup>  $R_f$  and  $R_{ct}$  values of NP-C electrode are determined to be 7.3 and 38.5  $\Omega$ , respectively, which are lower than the 21.8 and 57.9  $\Omega$  for the RGO electrode. The decreased  $R_{ct}$  in the NP-C electrode indicates rapid charge transfer, smaller polarization, and faster kinetics.<sup>47,48</sup> The superior rate performance, reversible capacity, and high CE of the NP-C electrodes can be explained by the synergistic effect of the heteroatom doping and stable host structure of the electrode. The 3D nanoarchitecture facilitates the access of the electrolyte as well as Li<sup>+</sup> diffusion. Meanwhile, the 3D porous structure not only provides more active surface sites for Li<sup>+</sup> storage but also better alleviates the stress from the volume change during cycling. N, P-codoping in the graphene layer produces a large number of defects, thereby enhancing the storage capacity of Li<sup>+</sup>. In addition, according to the report by Ma et al.,<sup>35</sup> P is more likely to integrate into the edge plane sites of the carbon material because of its larger atomic size. Therefore, the P atoms at the edge plane position are used to expand the interlayer distance to store more Li<sup>+</sup>, which helps enhance the Li<sup>+</sup> uptake.

To further evaluate the Li<sup>+</sup> diffusion coefficient in the NP-C electrode, the galvanostatic intermittent titration technique

(GITT) is performed (Figure S4). Figure 5a shows the potential response of mesoporous NP-C electrode during

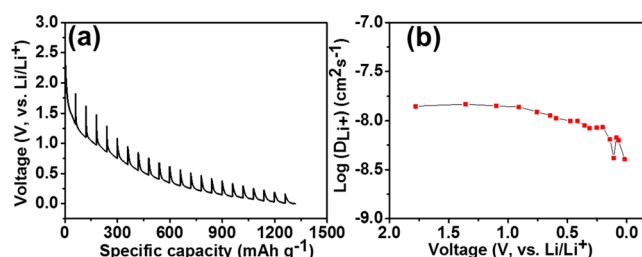


**Figure 5.** (a) GITT profile and (b) the lithium diffusion coefficients of NP-C calculated from GITT.

GITT measurement. The voltage profile for the NP-C electrode exhibits a gradual decrease during discharging (Li<sup>+</sup> insertion). Figure 5b shows the effective  $D_{Li^+}$  values when the electrode is discharged from 3 to 0.01 V. The diffusivity values at different voltages are on the same order of  $10^{-8}$  cm<sup>2</sup> s<sup>-1</sup>, which is larger than that of the graphite electrode.<sup>49,50</sup> It is clear that the diffusion associated with the sloping region (>0.3 V vs Li/Li<sup>+</sup>) is quite stable and occurs much faster than that of the plateau region (<~0.3 V), indicating enhanced Li<sup>+</sup> insertion into easily accessible sites, such as edges, defects, and pores in the carbon structure. Although the Li<sup>+</sup> diffusivity decreases in the plateau region (<~0.3 V), the values are still much higher than that of the graphite electrode, which benefits from the expanded interlayer distance by the N, P-codoping, leading to a faster Li<sup>+</sup> diffusion even within the interlayers. In addition, the sloping region contributes more capacity than that of the plateau region, which indicates that adsorption sites such as defects, pores, and edges have a significant role in Li<sup>+</sup> storage in the NP-C electrode.

The lithium storage mechanism is investigated by CV at various scan rates. As shown in Figure 6a, the typical CV response of the NP-C electrode is presented during the initial four cycles. From the first cycle, a broad peak is observed at

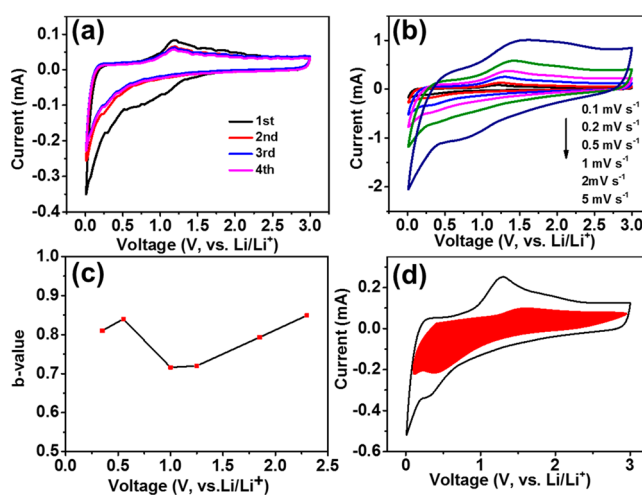


**Figure 6.** (a) Cyclic voltammograms of the NP-C electrode at a scan rate of 0.1 mV s<sup>-1</sup>. (b) Cyclic voltammograms of the NP-C electrode at various sweep rates from 0.1 to 5 mV s<sup>-1</sup>. (c)  $b$  values and voltammetric response (0.5 mV s<sup>-1</sup>). (d) Contribution of the capacitive current (red shaded area) to the overall cyclic voltammetry response at 0.5 mV s<sup>-1</sup>.

~0.75 V during the cathodic process, which disappears during the following cycles. This peak is mainly caused by the irreversible SEI layer formation. A second cathodic peak at ~0 V can be attributed to the Li<sup>+</sup> insertion into the carbon interlayers. Notably, the CV curves almost overlap from the second cycle, showing good stability and reversibility of the NP-C electrode. In the anodic scan, the peaks (at 0.25 and 1.25 V) are ascribed to the Li<sup>+</sup> extraction from layers and pores/defects of the carbon, respectively.<sup>51</sup> More micropores could be created when the phosphorus dopants interact with the graphene edges by forming C–O–P or C–P–O bonds and may serve as the adsorption sites to store Li<sup>+</sup> in the form of lithium clusters, thus enabling a high reversible specific capacity.<sup>52</sup> The CV results are consistent with the charge–discharge voltage profiles (Figure 4a).

The CV curves at different sweep rates from 0.1 to 5 mV s<sup>-1</sup> are shown in Figure 6b. The total electrochemical energy storage in the electrode can be ascribed into three mechanisms: diffusion-controlled faradaic intercalation process, the surface pseudocapacitive process, and the electrical double-layer effects. Based on the relationship between measured current (*i*) and sweep rate (*v*)<sup>53</sup>

$$i = av^b \quad (1)$$

the *i* is subject to a power law relationship with the scan rate *v*, where *a* and *b* are adjustable parameters. In particular, the *b* value could be obtained through calculating the slope of the log(*v*)–log(*i*) plots. The *b* value of 0.5 represents the diffusion-controlled behavior. When the *b* value is equal to 1, the charge storage is controlled by the capacitive behavior. The *b* values are calculated to be 0.72 at the anodic peak (Figure 6c), which suggests that the charge storage is controlled by both diffusion and capacitive processes. When potentials are higher or lower than the peak potential, the *b* value increases to 0.8–0.9, showing that the capacitive behavior dominates the overall charge storage. In addition, the diffusion and capacitive contribution to the current response can be quantitatively examined by the equation<sup>53</sup>

$$i = k_1v + k_2v^{1/2} \quad (2)$$

where the terms *k*<sub>1</sub>*v* and *k*<sub>2</sub>*v*<sup>1/2</sup> represent the contribution from surface capacitive effect and the diffusion-controlled process, respectively.<sup>54,55</sup> Through calculating *k*<sub>1</sub> and *k*<sub>2</sub> at each potential, the surface capacitance contribution can be obtained. In Figure 6d, the voltammetric response at a scan rate of 0.5 mV s<sup>-1</sup> shows that the capacitive contribution (red shaded area) is quite significant (67%) for the NP-C electrode. Because the capacitive contribution is involved in the process, we estimate that the surface area normalized capacitance is larger than that of a typical double-layer capacitor, 10–50 μF cm<sup>-2</sup>,<sup>56</sup> indicating the lithium storage mechanism on the surface is dominated by pseudocapacitive contribution. The significant capacitive contribution to the overall charge storage suggest that the defect sites at the carbon framework surface through N, P-codoping play a critical role in enhanced charge storage as well as fast kinetics of the NP-C electrode. The analysis of voltammetric responses at different scan rates suggests that the unique 3D porous carbon framework with ultrathin 2D layers facilitates surface redox reactions (pseudocapacitance), which enables fast charge storage and transfer kinetics for excellent rate capability.

## 4. CONCLUSION

In summary, the N, P-codoped carbon electrode (NP-C) is successfully synthesized through a strategic process using GO as backbones. The obtained NP-C electrode exhibits a good long-term cycling performance (740 mAh g<sup>-1</sup> after 2000 cycles at 2 A g<sup>-1</sup>), a relatively high initial Coulombic efficiency (74%), and excellent rate capability (e.g., 595 mA h g<sup>-1</sup> at 10 A g<sup>-1</sup>). Such excellent Li<sup>+</sup> storage and transport properties as well as the superb cycling stability of the NP-C can be explained by the following two factors: the 3D porous nanostructured carbon framework and the topological defects. The 3D porous nanostructured carbon framework can not only shorten the ion diffusion length by providing multidimensional interconnected pathways but also facilitate electrode/electrolyte contact and enhance fast charge transfer and transport. The topological defects and curled edges within the electrode create more active sites for Li<sup>+</sup> storage, leading to enhanced capacity due to pseudocapacitive contribution. Owing to the simple synthesis process, NP-C is a promising high-power and high-energy anode material for LIBs in large-scale applications. It is anticipated that this synthesis approach can stimulate the design of other new carbon composite materials for various storage systems.

## ■ ASSOCIATED CONTENT

### Supporting Information

The Supporting Information is available free of charge on the ACS Publications website at DOI: 10.1021/acsami.8b12302.

SEM of RGO and TEM images of the NP-C; C, N, and P EDX mapping; N<sub>2</sub> adsorption–desorption isotherm of NP-C; schematic of GITT technique and linear behavior of the *E* vs *τ*<sup>1/2</sup> relationship (PDF)

## ■ AUTHOR INFORMATION

### Corresponding Authors

\*E-mail: [clairexiong@boisestate.edu](mailto:clairexiong@boisestate.edu) (H.X.).

\*E-mail: [zfma@sjtu.edu.cn](mailto:zfma@sjtu.edu.cn) (Z.M.).

### ORCID

Hui Xiong: 0000-0003-3126-1476

### Notes

The authors declare no competing financial interest.

## ■ ACKNOWLEDGMENTS

This work was supported by the National Basic Research Program of China (2014CB239700), the National Natural Science Foundation of China (21336003, 21676165), the Shanghai Natural Science Foundation (15ZR1422300), and the College of Engineering of Boise State University. The authors appreciate Ms. P Skinner for proofreading the manuscript.

## ■ REFERENCES

- (1) Hassoun, J.; Panero, S.; Reale, P.; Scrosati, B. A New, Safe, High-Rate and High-Energy Polymer Lithium-Ion Battery. *Adv. Mater.* **2009**, *21*, 4807–4810.
- (2) Zhao, H.; Yang, Q.; Yuca, N.; Ling, M.; Higa, K.; Battaglia, V. S.; Parkinson, D. Y.; Srinivasan, V.; Liu, G. A Convenient and Versatile Method to Control the Electrode Microstructure toward High-Energy Lithium-Ion Batteries. *Nano Lett.* **2016**, *16*, 4686–4690.
- (3) Choi, J. W.; Aurbach, D. Promise and Reality of Post-Lithium-Ion Batteries with High Energy Densities. *Nat. Rev. Mater.* **2016**, *1*, 16013.

- (4) Zhang, J.; Liu, X. F.; Wang, J.; Shi, J. L.; Shi, Z. Q. Different Types of Pre-Lithiated Hard Carbon as Negative Electrode Material for Lithium-Ion Capacitors. *Electrochim. Acta* **2016**, *187*, 134–142.
- (5) Buiel, E.; George, A. E.; Dahn, J. R. On the Reduction of Lithium Insertion Capacity in Hard-Carbon Anode Materials with Increasing Heat-Treatment Temperature. *J. Electrochem. Soc.* **1998**, *145*, 2252–2257.
- (6) Chevallier, F.; Gautier, S.; Salvétat, J. P.; Clinard, C.; Frackowiak, E.; Rouzaud, J. N.; Beguin, F. Effects of Post-Treatments on the Performance of Hard Carbons in Lithium Cells. *J. Power Sources* **2001**, *97–98*, 143–145.
- (7) Luo, C.; Niu, S. Z.; Zhou, G. M.; Lv, W.; Li, B. H.; Kang, F. Y.; Yang, Q. H. Dual-Functional Hard Template Directed One-Step Formation of a Hierarchical Porous Carbon-Carbon Nanotube Hybrid for Lithium-Sulfur Batteries. *Chem. Commun.* **2016**, *52*, 12143–12146.
- (8) Huang, S. F.; Li, Z. P.; Wang, B.; Zhang, J. J.; Peng, Z. Q.; Qi, R. J.; Wang, J.; Zhao, Y. F. N-Doping and Defective Nanographitic Domain Coupled Hard Carbon Nanoshells for High Performance Lithium/Sodium Storage. *Adv. Funct. Mater.* **2018**, *28*, 1706294.
- (9) Cerbelaud, M.; Lestriez, B.; Ferrando, R.; Videcoq, A.; Richard-Plouet, M.; Caldes, M. T.; Guyomard, D. Numerical and Experimental Study of Suspensions Containing Carbon Blacks Used as Conductive Additives in Composite Electrodes for Lithium Batteries. *Langmuir* **2014**, *30*, 2660–2669.
- (10) Lee, J. H.; Wee, S. B.; Kwon, M. S.; Kim, H. H.; Choi, J. M.; Song, M. S.; Park, H. B.; Kim, H.; Paik, U. Strategic Dispersion of Carbon Black and Its Application to Ink-Jet-Printed Lithium Cobalt Oxide Electrodes for Lithium Ion Batteries. *J. Power Sources* **2011**, *196*, 6449–6455.
- (11) Chen, Z. H.; Christensen, L.; Dahn, J. R. Mechanical and Electrical Properties of Poly(Vinylidene Fluoride-Tetrafluoroethylene-Propylene)/Super-S Carbon Black Swelled in Liquid Solvent as an Electrode Binder for Lithium-Ion Batteries. *J. Appl. Polym. Sci.* **2004**, *91*, 2958–2965.
- (12) Liu, Y. H.; Takasaki, T.; Nishimura, K.; Yanagida, M.; Sakai, T. Development of Lithium Ion Battery Using Fiber-Type Lithium-Rich Cathode and Carbon Anode Materials. *J. Power Sources* **2015**, *290*, 153–158.
- (13) Lyu, H. L.; Liu, J. R.; Qiu, S.; Cao, Y. H.; Hu, C. X.; Guo, S. M.; Guo, Z. H. Carbon Composite Spun Fibers with in Situ Formed Multicomponent Nanoparticles for a Lithium-Ion Battery Anode with Enhanced Performance. *J. Mater. Chem. A* **2016**, *4*, 9881–9889.
- (14) Yang, Z. W.; Guo, H. J.; Li, X. H.; Wang, Z. X.; Yan, Z. L.; Wang, Y. S. Natural Sisal Fibers Derived Hierarchical Porous Activated Carbon as Capacitive Material in Lithium Ion Capacitor. *J. Power Sources* **2016**, *329*, 339–346.
- (15) Tian, Q. H.; Zhang, Z. X.; Yang, L.; Hirano, S. Three-Dimensional Wire-in-Tube Hybrids of Tin Dioxide and Nitrogen-Doped Carbon for Lithium Ion Battery Applications. *Carbon* **2015**, *93*, 887–895.
- (16) Liu, Y.; Yan, X. D.; Yu, Y. H.; Yang, X. P. Self-Improving Anodes for Lithium-Ion Batteries: Continuous Interlamellar Spacing Expansion Induced Capacity Increase in Polydopamine-Derived Nitrogen-Doped Carbon Tubes During Cycling. *J. Mater. Chem. A* **2015**, *3*, 20880–20885.
- (17) Xu, Y. J.; Liu, X.; Cui, G. L.; Zhu, B.; Weinberg, G.; Schlogl, R.; Maier, J.; Su, D. S. A Comparative Study on the Lithium-Ion Storage Performances of Carbon Nanotubes and Tube-in-Tube Carbon Nanotubes. *ChemSusChem* **2010**, *3*, 343–349.
- (18) Hou, Y.; Li, J. Y.; Wen, Z. H.; Cui, S. M.; Yuan, C.; Chen, J. H. N-Doped Graphene/Porous G-C<sub>3</sub>N<sub>4</sub> Nanosheets Supported Layered-MoS<sub>2</sub> Hybrid as Robust Anode Materials for Lithium-Ion Batteries. *Nano Energy* **2014**, *8*, 157–164.
- (19) Su, Y. Z.; Liu, Y. X.; Liu, P.; Wu, D. Q.; Zhuang, X. D.; Zhang, F.; Feng, X. L. Compact Coupled Graphene and Porous Polyaryltriazine-Derived Frameworks as High Performance Cathodes for Lithium-Ion Batteries. *Angew. Chem., Int. Ed.* **2015**, *54*, 1812–1816.
- (20) Zhang, Y.; Chen, P. H.; Gao, X.; Wang, B.; Liu, H.; Wu, H.; Liu, H. K.; Dou, S. X. Nitrogen-Doped Graphene Ribbon Assembled Core-Sheath MnO@Graphene Scrolls as Hierarchically Ordered 3d Porous Electrodes for Fast and Durable Lithium Storage. *Adv. Funct. Mater.* **2016**, *26*, 7754–7765.
- (21) Sui, Z.-Y.; Wang, C.; Yang, Q.-S.; Shu, K.; Liu, Y.-W.; Han, B.-H.; Wallace, G. G. A Highly Nitrogen-Doped Porous Graphene - an Anode Material for Lithium Ion Batteries. *J. Mater. Chem. A* **2015**, *3*, 18229–18237.
- (22) Zhang, J.; Yang, Z.; Qiu, J.; Lee, H.-W. Design and Synthesis of Nitrogen and Sulfur Co-Doped Porous Carbon Via Two-Dimensional Interlayer Confinement for a High-Performance Anode Material for Lithium-Ion Batteries. *J. Mater. Chem. A* **2016**, *4*, 5802–5809.
- (23) Liu, X. X.; Chao, D. L.; Li, Y.; Hao, J.; Liu, X. S.; Zhao, J. P.; Lin, J. Y.; Fan, H. J.; Shen, Z. X. A Low-Cost and One-Step Synthesis of N-Doped Monolithic Quasi-Graphene Films with Porous Carbon Frameworks for Li-Ion Batteries. *Nano Energy* **2015**, *17*, 43–51.
- (24) Tabassum, H.; Zou, R. Q.; Mahmood, A.; Liang, Z. B.; Wang, Q. F.; Zhang, H.; Gao, S.; Qu, C.; Guo, W. H.; Guo, S. J. A Universal Strategy for Hollow Metal Oxide Nanoparticles Encapsulated into B/N Co-Doped Graphitic Nanotubes as High-Performance Lithium-Ion Battery Anodes. *Adv. Mater.* **2018**, *30*, 1705441.
- (25) Khanra, A.; Sangam, S.; Shakeel, A.; Suhag, D.; Mistry, S.; Rai, M. P.; Chakrabarti, S.; Mukherjee, M. Sustainable Growth and Lipid Production from *Chlorella Pyrenoidosa* Using N-Doped Carbon Nanosheets: Unravelling the Role of Graphitic Nitrogen. *ACS Sustainable Chem. Eng.* **2018**, *6*, 774–780.
- (26) Qin, W. W.; Teng, Y. Q.; Zhang, J. K.; Xiao, X. F.; Li, Y.; Li, Z. Y. Sandwich-Like Nanosheets of a N-Doped Porous Carbon/Graphene Composite with Enhanced Electrochemical Properties for Lithium and Sodium Storage. *ChemElectroChem.* **2018**, *5*, 694–700.
- (27) Lee, J.; Park, S. K.; Piao, Y. N-Doped Carbon Framework/Reduced Graphene Oxide Nanocomposite as a Sulfur Reservoir for Lithium-Sulfur Batteries. *Electrochim. Acta* **2016**, *222*, 1345–1353.
- (28) Li, X. Y.; Fu, N. Q.; Zou, J. Z.; Zeng, X. R.; Chen, Y. M.; Zhou, L. M.; Huang, H. T. Sulfur-Impregnated N-Doped Hollow Carbon Nanofibers as Cathode for Lithium-Sulfur Batteries. *Mater. Lett.* **2017**, *209*, 505–508.
- (29) Tan, G.; Bao, W.; Yuan, Y.; Liu, Z.; Shahbazian-Yassar, R.; Wu, F.; Amine, K.; Wang, J.; Lu, J. Freestanding Highly Defect Nitrogen-Enriched Carbon Nanofibers for Lithium Ion Battery Thin-Film Anodes. *J. Mater. Chem. A* **2017**, *5*, 5532–5540.
- (30) Wang, S. Q.; Xia, L.; Yu, L.; Zhang, L.; Wang, H. H.; Lou, X. W. Free-Standing Nitrogen-Doped Carbon Nanofiber Films: Integrated Electrodes for Sodium-Ion Batteries with Ultralong Cycle Life and Superior Rate Capability. *Adv. Energy Mater.* **2016**, *6*, 1502217.
- (31) Hummers, W. S.; Offeman, R. E. Preparation of Graphitic Oxide. *J. Am. Chem. Soc.* **1958**, *80*, 1339.
- (32) Kim, T.-H.; Jeon, E. K.; Ko, Y.; Jang, B. Y.; Kim, B.-S.; Song, H.-K. Enlarging the D-Spacing of Graphite and Polarizing Its Surface Charge for Driving Lithium Ions Fast. *J. Mater. Chem. A* **2014**, *2*, 7600–7605.
- (33) Hankel, M.; Searles, D. J. Lithium Storage on Carbon Nitride, Graphynylene and Inorganic Graphynylene. *Phys. Chem. Chem. Phys.* **2016**, *18*, 14205–14215.
- (34) Yang, J. Q.; Zhou, X. L.; Wu, D. H.; Zhao, X. D.; Zhou, Z. S-Doped N-Rich Carbon Nanosheets with Expanded Interlayer Distance as Anode Materials for Sodium-Ion Batteries. *Adv. Mater.* **2017**, *29*, 1604108.
- (35) Ma, X. L.; Ning, G. Q.; Qi, C. L.; Xu, C. G.; Gao, J. S. Phosphorus and Nitrogen Dual-Doped Few-Layered Porous Graphene: A High-Performance Anode Material for Lithium-Ion Batteries. *ACS Appl. Mater. Interfaces* **2014**, *6*, 14415–14422.
- (36) Li, Y.; Yuan, Y.; Bai, Y.; Liu, Y.; Wang, Z.; Li, L.; Wu, F.; Amine, K.; Wu, C.; Lu, J. Insights into the Na<sup>+</sup> Storage Mechanism of Phosphorus-Functionalized Hard Carbon as Ultrahigh Capacity Anodes. *Adv. Energy Mater.* **2018**, *8*, 1702781.

- (37) Zhang, J. T.; Qu, L. T.; Shi, G. Q.; Liu, J. Y.; Chen, J. F.; Dai, L. M. N. P-Codoped Carbon Networks as Efficient Metal-Free Bifunctional Catalysts for Oxygen Reduction and Hydrogen Evolution Reactions. *Angew. Chem., Int. Ed.* **2016**, *55*, 2230–2234.
- (38) Wu, H. L.; Xia, L.; Ren, J.; Zheng, Q. J.; Xu, C. G.; Lin, D. M. A High-Efficiency N/P Co-Doped Graphene/Cnt@Porous Carbon Hybrid Matrix as a Cathode Host for High Performance Lithium-Sulfur Batteries. *J. Mater. Chem. A* **2017**, *5*, 20458–20472.
- (39) Guan, J.; Zhong, X. W.; Chen, X.; Zhu, X. J.; Li, P. L.; Wu, J. H.; Lu, Y. L.; Yu, Y.; Yang, S. F. Expanding Pore Sizes of Zif-8-Derived Nitrogen-Doped Microporous Carbon Via C-60 Embedding: Toward Improved Anode Performance for the Lithium-Ion Battery. *Nanoscale* **2018**, *10*, 2473–2480.
- (40) Fromm, O.; Heckmann, A.; Rodehorst, U. C.; Frerichs, J.; Becker, D.; Winter, M.; Placke, T. Carbons from Biomass Precursors as Anode Materials for Lithium Ion Batteries: New Insights into Carbonization and Graphitization Behavior and into Their Correlation to Electrochemical Performance. *Carbon* **2018**, *128*, 147–163.
- (41) Huang, Y. S.; Li, K.; Yang, G. H.; Aboud, M. F. A.; Shakir, I.; Xu, Y. X. Ultrathin Nitrogen-Doped Carbon Layer Uniformly Supported on Graphene Frameworks as Ultrahigh-Capacity Anode for Lithium-Ion Full Battery. *Small* **2018**, *14*, 1703969.
- (42) Zhu, K. J.; Liu, J.; Li, S. T.; Liu, L. L.; Yang, L. Y.; Liu, S. L.; Wang, H.; Xie, T. Ultrafine Cobalt Phosphide Nanoparticles Embedded in Nitrogen-Doped Carbon Matrix as a Superior Anode Material for Lithium Ion Batteries. *Adv. Mater. Interfaces* **2017**, *4*, 1700377.
- (43) Qiu, Z. Z.; Lin, Y. M.; Xin, H. L.; Han, P.; Li, D. Z.; Yang, B.; Li, P. C.; Ullah, S.; Fan, H. S.; Zhu, C. Z.; Xu, J. Ultrahigh Level Nitrogen/Sulfur Co-Doped Carbon as High Performance Anode Materials for Lithium-Ion Batteries. *Carbon* **2018**, *126*, 85–92.
- (44) Long, B.; Balogun, M. S.; Luo, L.; Luo, Y.; Qiu, W. T.; Song, S. Q.; Zhang, L.; Tong, Y. X. X. Encapsulated Vanadium-Based Hybrids in Amorphous N-Doped Carbon Matrix as Anode Materials for Lithium-Ion Batteries. *Small* **2017**, *13*, 1702081.
- (45) Zhang, J.; Yang, Z. X.; Qiu, J. Y. C.; Lee, H. W. Design and Synthesis of Nitrogen and Sulfur Co-Doped Porous Carbon Via Two-Dimensional Interlayer Confinement for a High-Performance Anode Material for Lithium-Ion Batteries. *J. Mater. Chem. A* **2016**, *4*, 5802–5809.
- (46) Aurbach, D.; Markovsky, B.; Weissman, I.; Levi, E.; Ein-Eli, Y. On the Correlation between Surface Chemistry and Performance of Graphite Negative Electrodes for Li Ion Batteries. *Electrochim. Acta* **1999**, *45*, 67–86.
- (47) Hu, M. X.; Zhou, H. J.; Gan, X.; Yang, L.; Huang, Z. H.; Wang, D. W.; Kang, F. Y.; Lv, R. T. Ultrahigh Rate Sodium Ion Storage with Nitrogen-Doped Expanded Graphite Oxide in Ether-Based Electrolyte. *J. Mater. Chem. A* **2018**, *6*, 1582–1589.
- (48) Ou, J. K.; Yang, L.; Zhang, Z.; Xi, X. H. Honeysuckle-Derived Hierarchical Porous Nitrogen, Sulfur, Dual-Doped Carbon for Ultra-High Rate Lithium Ion Battery Anodes. *J. Power Sources* **2016**, *333*, 193–202.
- (49) Verma, P.; Maire, P.; Novák, P. A Review of the Features and Analyses of the Solid Electrolyte Interphase in Li-Ion Batteries. *Electrochim. Acta* **2010**, *55*, 6332–6341.
- (50) Markevich, E.; Levi, M. D.; Aurbach, D. Comparison between Potentiostatic and Galvanostatic Intermittent Titration Techniques for Determination of Chemical Diffusion Coefficients in Ion-Insertion Electrodes. *J. Electroanal. Chem.* **2005**, *580*, 231–237.
- (51) Chen, J. J.; Mao, Z. Y.; Zhang, L. X.; Wang, D. J.; Xu, R.; Bie, L. J.; Fahlman, B. D. Nitrogen-Deficient Graphitic Carbon Nitride with Enhanced Performance for Lithium Ion Battery Anodes. *ACS Nano* **2017**, *11*, 12650–12657.
- (52) Tao, H. C.; Xiong, L. Y.; Du, S. L.; Zhang, Y. Q.; Yang, X. L.; Zhang, L. L. Interwoven N and P Dual-Doped Hollow Carbon Fibers/Graphitic Carbon Nitride: An Ultrahigh Capacity and Rate Anode for Li and Na Ion Batteries. *Carbon* **2017**, *122*, 54–63.
- (53) Wang, J.; Polleux, J.; Lim, J.; Dunn, B. Pseudocapacitive Contributions to Electrochemical Energy Storage in TiO<sub>2</sub> (Anatase) Nanoparticles. *J. Phys. Chem. C* **2007**, *111*, 14925–14931.
- (54) Bachman, J. C.; Kaviani, R.; Graham, D. J.; Kim, D. Y.; Noda, S.; Nocera, D. G.; Shao-Horn, Y.; Lee, S. W. Electrochemical Polymerization of Pyrene Derivatives on Functionalized Carbon Nanotubes for Pseudocapacitive Electrodes. *Nat. Commun.* **2015**, *6*, 7040.
- (55) Shen, L. F.; Lv, H. F.; Chen, S. Q.; Kopold, P.; van Aken, P. A.; Wu, X. J.; Maier, J.; Yu, Y. Peapod-Like Li<sub>3</sub>VO<sub>4</sub>/N-Doped Carbon Nanowires with Pseudocapacitive Properties as Advanced Materials for High-Energy Lithium-Ion Capacitors. *Adv. Mater.* **2017**, *29*, 1700142.
- (56) Conway, B. E.; Birss, V.; Wojtowicz, J. The Role and Utilization of Pseudocapacitance for Energy Storage by Supercapacitors. *J. Power Sources* **1997**, *66*, 1–14.